



# Characterization of Iron Precipitates in a SAPS Limestone Layer for Flushing System Design

Dong-kil Lee<sup>1</sup> · Seung-wook Shin<sup>1</sup> · Young-wook Cheong<sup>1</sup>

Received: 21 July 2017 / Accepted: 2 April 2018 / Published online: 3 April 2018  
© Springer-Verlag GmbH Germany, part of Springer Nature 2018

## Abstract

In successive alkalinity-producing systems (SAPS), the limestone tends to get coated with precipitates, reducing the permeability of the SAPS, the mine water treatment efficiency, and the service life of the SAPS. Further study of the precipitates are required to improve the design of flushing systems. In this study, the growth characteristics, particle size distribution, and chemical composition of these precipitates were determined. Based on their growth characteristics, precipitates were classified into four types, and the critical velocity of the precipitates, which is a design parameter of flushing systems, was evaluated through experiments. The resulting critical velocity was used to identify the minimum number of orifices required for lateral pipes in flushing systems.

**Keywords** Acid mine drainage · SEM-EDS · Particle size distribution · Critical velocity

## Introduction

Acid mine drainage (AMD) is generated when rock containing pyrite is exposed to air and water. The low pH (4.5 or less) and metal content of the resulting AMD can cause severe water and soil contamination (Akcil and Koldas 2006). Active treatment methods that precipitate and purify pollutants by increasing the pH of AMD are effective, but may not be economically feasible because AMD occurs over various extents and time periods. In contrast, passive treatment methods, such as successive alkalinity-producing systems (SAPS), anoxic limestone drains (ALDs), and constructed wetlands, have an extended operational lifespan, and, despite relatively high installation costs, is typically economical for long-term operations (Christensen et al. 1996; Cravotta 2008; Hedin et al. 1994; Jarvis and Laine 2003; Wolkersdorfer et al. 2005; Younger 2000; Younger et al. 2002).

SAPS (Kepler and McCleary 1997) is a passive treatment method in which contaminated water is treated as it passes through a layer of organic matter and porous limestone. However, a drawback of SAPS as well as other passive

treatment methods is that precipitates can be deposited in the pores of the limestone layers, deteriorating permeability and treatment capacity (Ford 2003). Watson et al. (2009) and Taylor et al. (2016) demonstrated this permeability deterioration over time using tracer tests. Flushing systems, such as proposed by Danehy et al. (2002), address such permeability problems by periodically eliminating these precipitates. Weaver et al. (2004) found that the precipitates should be flushed away every 4 weeks. However, if the interval between the removal cycles is too long, the particles grow larger and solidify, hindering their removal. Several studies have focused on evaluating SAPS and improving their performance (Bhattacharya et al. 2008; Lee et al. 2013; Watzlaf et al. 2002; Yim et al. 2015).

Short-circuiting of AMD in a SAPS may occur due to construction defects and thin or inhomogeneous organic matter in the SAPS. Zones near these short circuits showed an increase in red Fe-oxide stains, suggesting an oxidizing environment within or below the compost matter (Rose 2004, 2006). Demchak et al. (2001) found that the distribution of oxidation and reduction in the organic layer was not uniform in the SAPS's they studied, due to heterogeneous flow and short-circuiting. Additionally, deeply oxidized zones substantiated observations that channelized flow was occurring. In a field survey of SAPS's in Korea, iron oxides were identified in effluents issuing from the outlets of SAPS's, and on the surface of limestone excavated during repair of SAPS's.

✉ Dong-kil Lee  
ldk@kigam.re.kr

<sup>1</sup> Korea Institute Geoscience and Mineral Resources (KIGAM), 124 Gwahang-no, Yuseong-gu, Daejeon 34132, South Korea

Most of the precipitates occurring in the limestone layer in the SAPS are aluminum compounds (Skousen et al. 2017), but in SAPS's with short circuiting, iron precipitates may occur. The iron that accumulates in the organic material (Rose 2004) may flow into the limestone layer during flushing. Few studies have characterized these the iron and aluminum precipitates, even though this is important for flushing system optimization.

This study focused on the iron precipitates and characterized the precipitates generated in limestone layers at different growth stages. In addition, because it is an important design factor in flushing systems, the critical velocity of precipitates was measured in laboratory experiments performed on various iron oxide types.

## Materials and methods

### Precipitation experiment

The precipitate growth test to identify the physicochemical characteristics of the AMD precipitates was performed at a passive treatment facility located near the Samma–Taejung mine at Samcheok, Gangwon province in northeastern South Korea (Fig. 1). Table 1 shows the AMD characteristics measured, which included pH, electrical conductivity (EC), total dissolved solids (TDS), salinity, and turbidity. The pH of the Samma–Taejung mine drainage was acidic (3.5) and

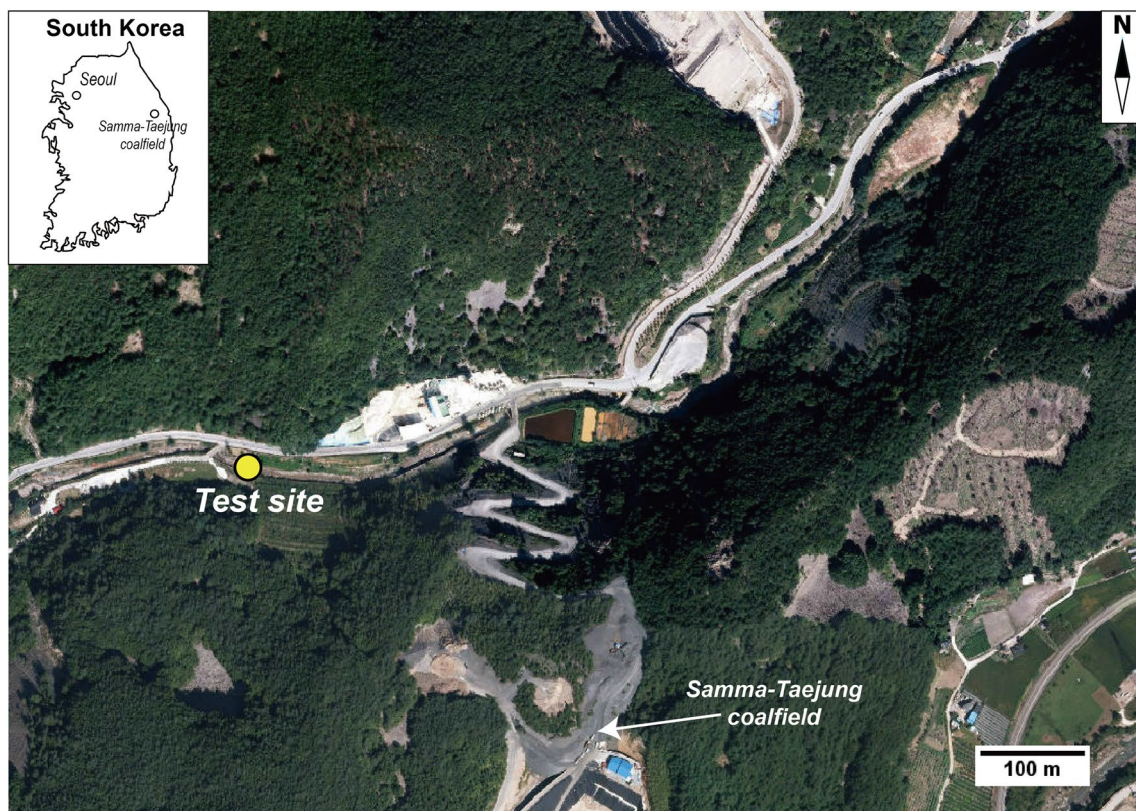


Fig. 1 Satellite image of the test site for the iron-oxide precipitation experiment near Samma–Taejung coalfield (Naver 2016)

Table 1 Properties of AMD from the Samma–Taejung coalfield

Parameter	Value	Parameter	Value
pH	3.5	Dissolved oxygen (DO)	3.32 mg/L
Electrical conductivity (EC)	3.26 mS cm <sup>-1</sup>	Oxidation–reduction potential (ORP)	365.8 mV
Total dissolved solids (TDS)	1676 mg/L	Ferrous concentration	215 mg/L
Salinity	1.71‰	Total iron content	228 mg/L
Turbidity	0.74 NTU	Temperature	16.7 °C
Al concentration	80.3 mg/L	SO <sub>4</sub> <sup>2-</sup> concentration	2,500 mg/L



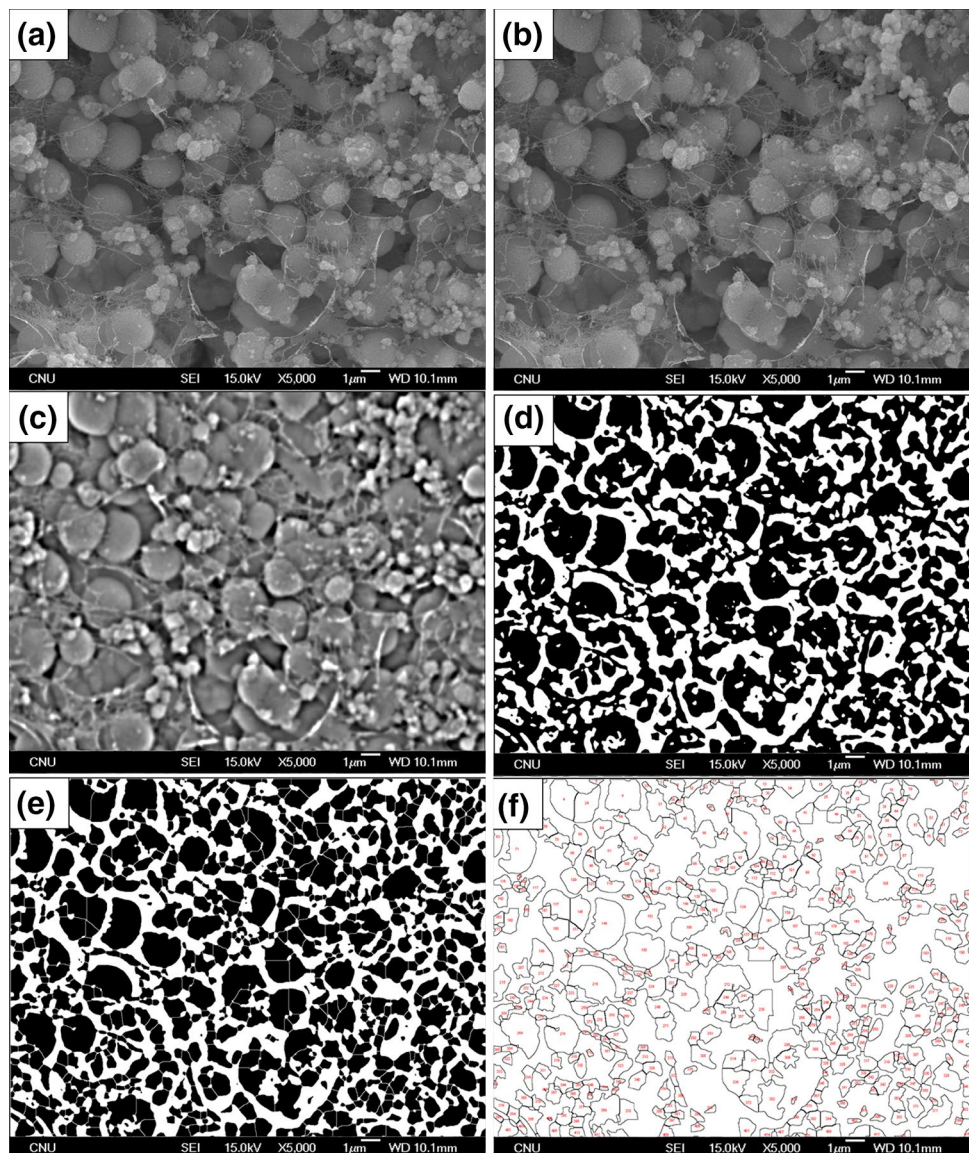
its Fe(II) ion content was 215 mg/L (Table 1), exceeding Korea's effluent standard (7 mg/L).

To monitor precipitate characteristics over time, 600 g of limestone aggregate, with a mean particle size of 25.4 mm, was washed with water and added to six 500 mL beakers, which were then fully submerged in the mine drainage. As the beakers were placed in a continuous stream of AMD, the characteristics of the AMD were almost constant. One beaker was removed periodically each week over the course of 6 weeks to visually identify the precipitate characteristics. The particle size of the precipitates was measured using a Malvern Mastersizer 2000 analyzer. Particle distribution was then classified and the change in particle distribution over time was examined.

The precipitates were classified into several types based on their appearance. The chemical composition

of each type of precipitate and the micro-scale characteristics of the particles were identified using a scanning electron microscopy with energy dispersive spectroscopy (SEM-EDS) analysis. Changes in precipitate grain size were quantitatively analyzed in SEM images using Image J software. The SEM image analysis procedure is summarized in Fig. 2. An area for grain size analysis was selected (Fig. 2b) from the SEM image shown in Fig. 2a and filtered using an FFT-based band pass filter (Fig. 2c). Grains and pores were distinguished in the filtered images using a threshold function (Fig. 2d). The grain boundaries were determined using the closed and watershed functions (Fig. 2e). Grain sizes were automatically calculated using the particle analysis function (Fig. 2f). To measure precipitate density, precipitate samples were dried and then measured using a pycnometer.

**Fig. 2** Grain size analysis using SEM images and the Image J software. **a** SEM image of precipitate, **b** analysis area selection, **c** bandpass filter processing based on the fast Fourier transform (FFT) algorithm, **d** processing threshold phase, **e** grain boundary determination, and **f** grain size analysis



### Laboratory Critical Velocity Measurement

To ensure that an iron precipitate is effectively discharged from a limestone layer, the AMD velocity in the flushing system must be greater than the critical velocity at which precipitates start to move by water flow. Thus, determining the critical velocity of the precipitates is essential when designing a flushing system. For this reason, a critical velocity measurement system was designed to measure the critical velocity of precipitates in the flushing pipe. This measurement system consists of a stand, a clear acrylic cylinder, a sample injector, a water pump, and a water tank (Fig. 3).

First, the cylinder was attached horizontally to the stand and filled with water using the pump. The valves on both

precipitates moved. The equivalent diameters of the precipitate particles used in the experiment are shown in Table 3; the average density of the precipitates was  $2.50 \text{ g cm}^{-3}$ .

The critical velocity of particles can be calculated using empirical equations. Equation 1 was suggested by Thomas (1979) for grain sizes  $< 100 \text{ }\mu\text{m}$  and Eq. 2 was introduced by Oroskar and Turian (1980) for grain sizes  $> 100 \text{ }\mu\text{m}$ . The experimental results were compared to the calculations undertaken to determine the critical velocity appropriate for an optimum flushing system.

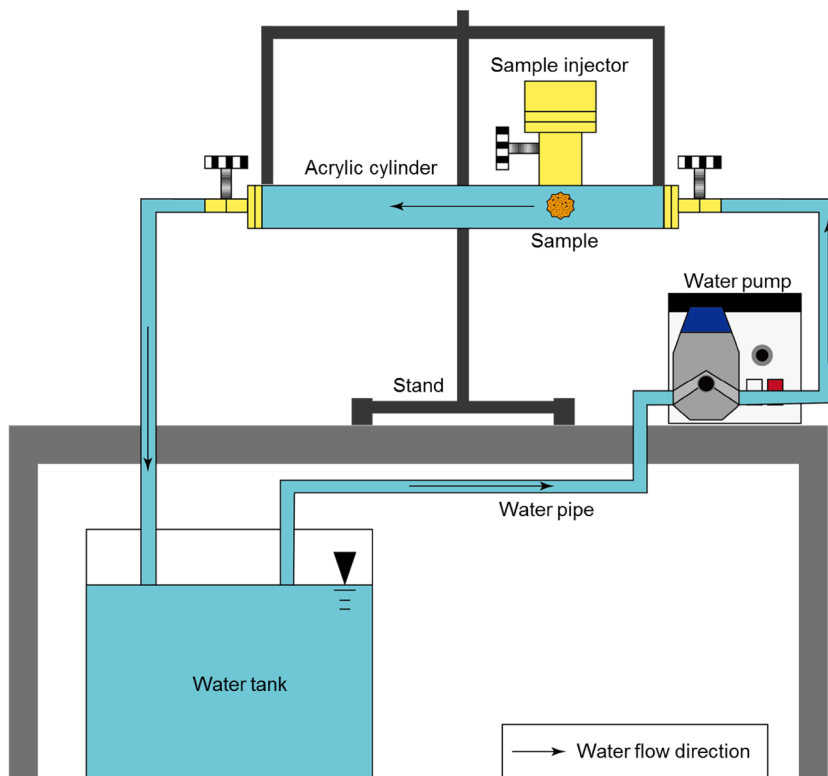
$$v_c = 9.0 \left( \frac{g\mu(s-1)}{\rho_l} \right)^{0.37} \left( \frac{D\rho_l}{\mu} \right)^{0.11} \tag{1}$$

$$v_c = \sqrt{gd(s-1)} \left[ 1.85C^{0.1536}(1-C)^{0.3564} \left( \frac{D}{d} \right)^{0.378} \left( \frac{\rho_l D \sqrt{gd(s-1)}}{\mu} \right)^{0.09} x^{0.3} \right] \tag{2}$$

sides of the cylinder were closed so that the water would remain still. The precipitate, separated by a knife and dried, was then injected into the cylinder using the sample injector installed atop of the cylinder. The valves on both sides of the cylinder were then opened, and the water flow rate was slowly increased by adjusting the pump. The critical velocity was identified as the water flow rate at the point at which the

where,  $v_c$  is the critical velocity of the slurry (m/s),  $g$  is the gravitational acceleration ( $9.806 \text{ m/s}^2$ ),  $D$  is the internal diameter of the pipe (m),  $d$  is the diameter of a particle (m),  $s$  is the density ratio of solid to liquid,  $C$  is the solid concentration (volume fraction),  $\rho_l$  is the density of the liquid ( $\text{kg m}^{-3}$ ),  $\mu$  is the kinematic coefficient of viscosity of water (Pa-s), and  $\chi$  is the hindered settling factor.

**Fig. 3** Laboratory critical velocity measurement system for precipitates





## Results and Discussion

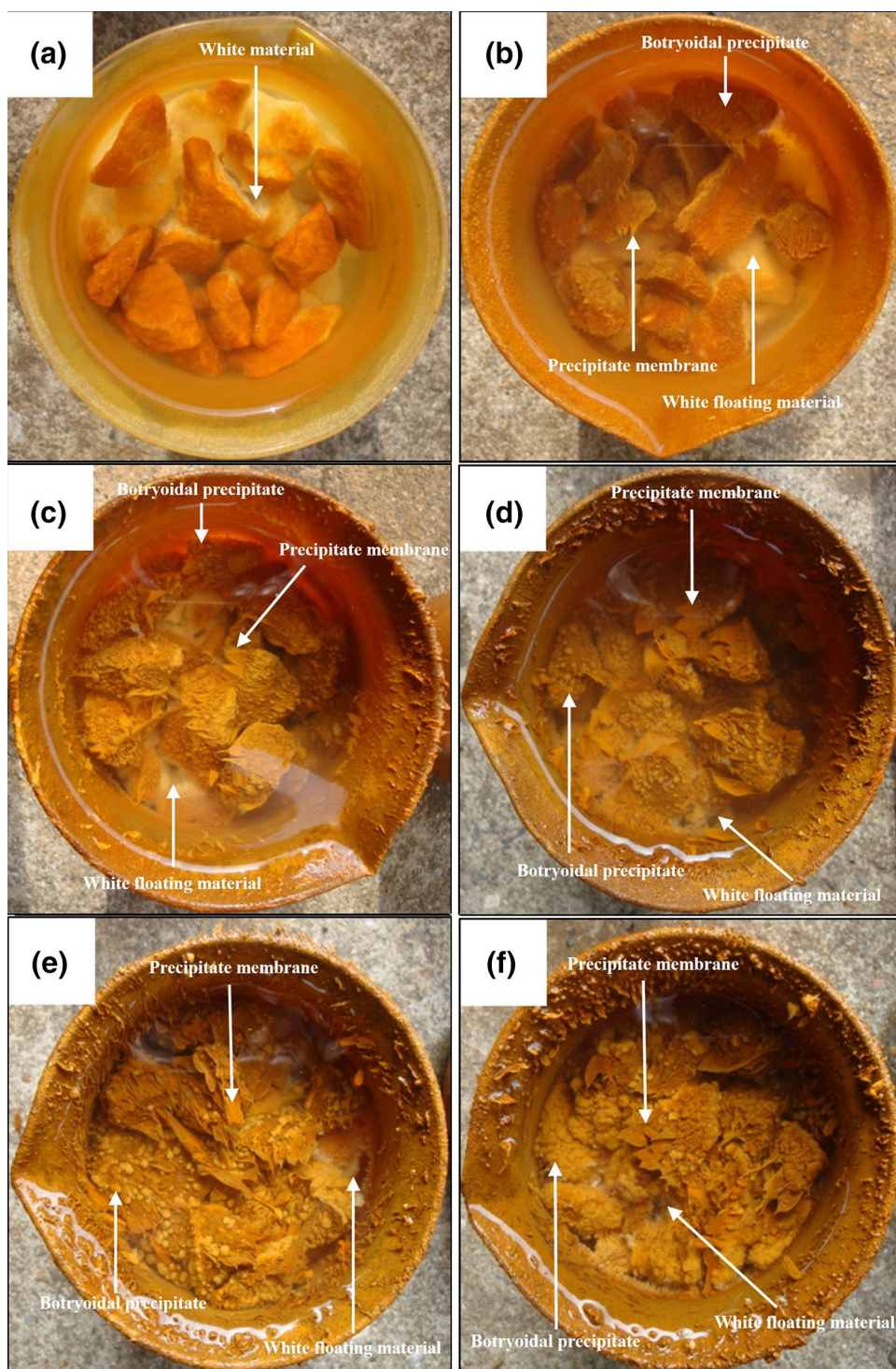
### Visual Inspection

Figure 4 shows the limestone aggregate specimens obtained from the precipitate growth tests. The precipitates

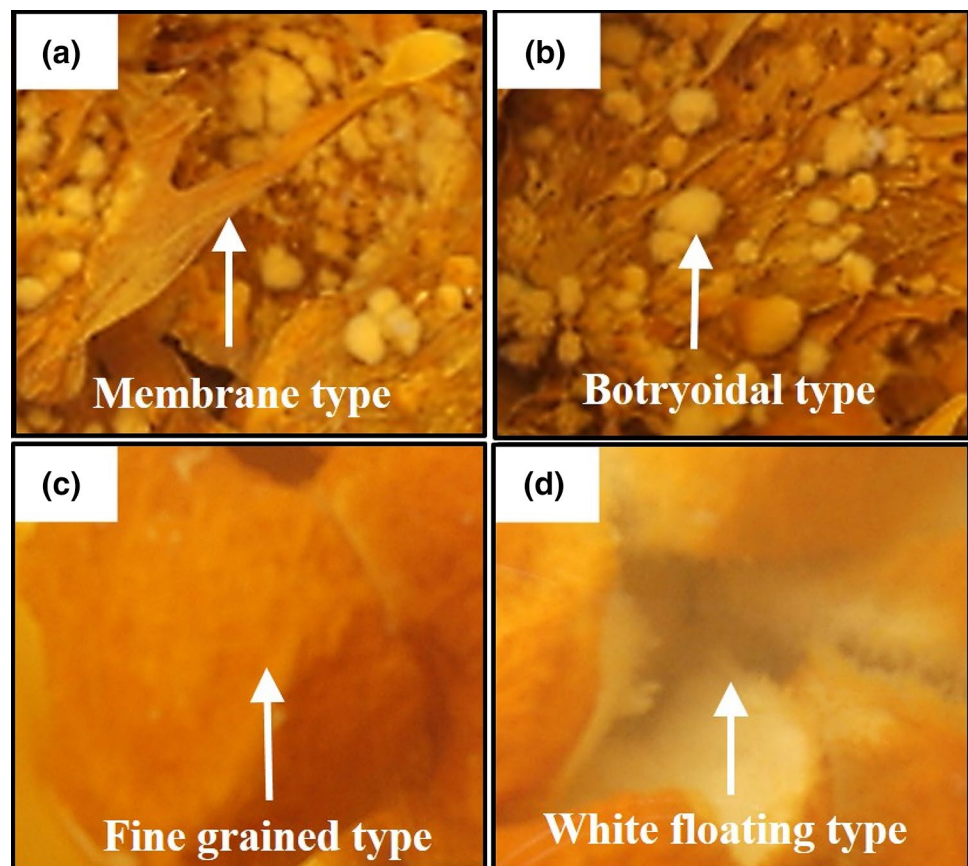
were classified into membrane, botryoidal, fine-grained, and white floating types (Fig. 5).

As shown in Fig. 4a, the surface of the limestone in the 1-week beaker was covered with a thin layer of yellow material and a floating white material appeared around the uncoated limestone. Figure 4b shows that after 2 weeks, botryoidal precipitates approximately 0.5 mm in diameter

**Fig. 4** Images of samples used in the six-week precipitation experiment; samples after **a** 1 week, **b** 2 weeks, **c** 3 weeks, **d** 4 weeks, **e** 5 weeks, and **f** 6 weeks



**Fig. 5** Images of representative precipitates observed in the samples; **a** membrane type, **b** botryoidal type, **c** fine-grained type, and **d** white floating type



appeared on the flat surfaces of the limestone aggregate, and a thin precipitate membrane of 2–3 mm (max. 5 mm) width appeared at the edges (or apical ends) of the limestone surface. Approximately 80% of the upper portion of the limestone surface was covered by precipitates and white floating material was present. Figure 4c shows the samples after three weeks; the precipitate membrane size had grown to 10 mm long and 7–8 mm wide, and moved following the direction of water flow, meaning that it was not in a solid state. The botryoidal precipitates were present in greater quantities and their diameter was now 1.5 mm. Gradually, white material also appeared in the lower part of the uncoated limestone layer. Figure 4d shows the appearance of the samples after four weeks. The size of the precipitate membrane had increased to 18 mm in length and 10 mm in width. It was soft, and fragmented when even slightly touched. The diameter of the botryoidal precipitates had increased to 2–2.5 mm. Figure 4e shows the appearance of the samples after 5 weeks. The size of the precipitate membrane had decreased to 13 mm in length and 5 mm in width. Although it fragmented when touched, a portion remained, meaning that it was gradually hardening. The diameter of the botryoidal precipitates had increased to 2.5–4 mm. Figure 4f shows the appearance of the samples after 6 weeks. During this week, the size of the precipitate membrane had

decreased to 8–10 mm in length and 5 mm in width, indicating that the membrane was becoming progressively harder. The diameter of the botryoidal precipitates had increased to 4 mm and they had merged with adjacent botryoidal precipitates to form a single mass. The precipitate membrane reached its largest size during the fourth week, after which it gradually hardened.

Initially, the precipitate was light brown, which gradually changed to dark brown as the precipitate solidified. The floating white material moved from the upper part of the limestone layer to the lower part as the upper part became coated by precipitates. Membranous precipitates were predominant during the early stage of the experiment, while botryoidal precipitates were predominant during the late stage.

### Grain Size Analysis

Figure 6 presents the results of the grain size analysis and shows the change in the grain size of the precipitates in the limestone layers over time. Figure 6a shows the grain size distribution after the limestone had been immersed for one week in the mine drainage. The grain size distribution was divided into four groups. Group G1 included precipitates generated during the early stage of the experiment;



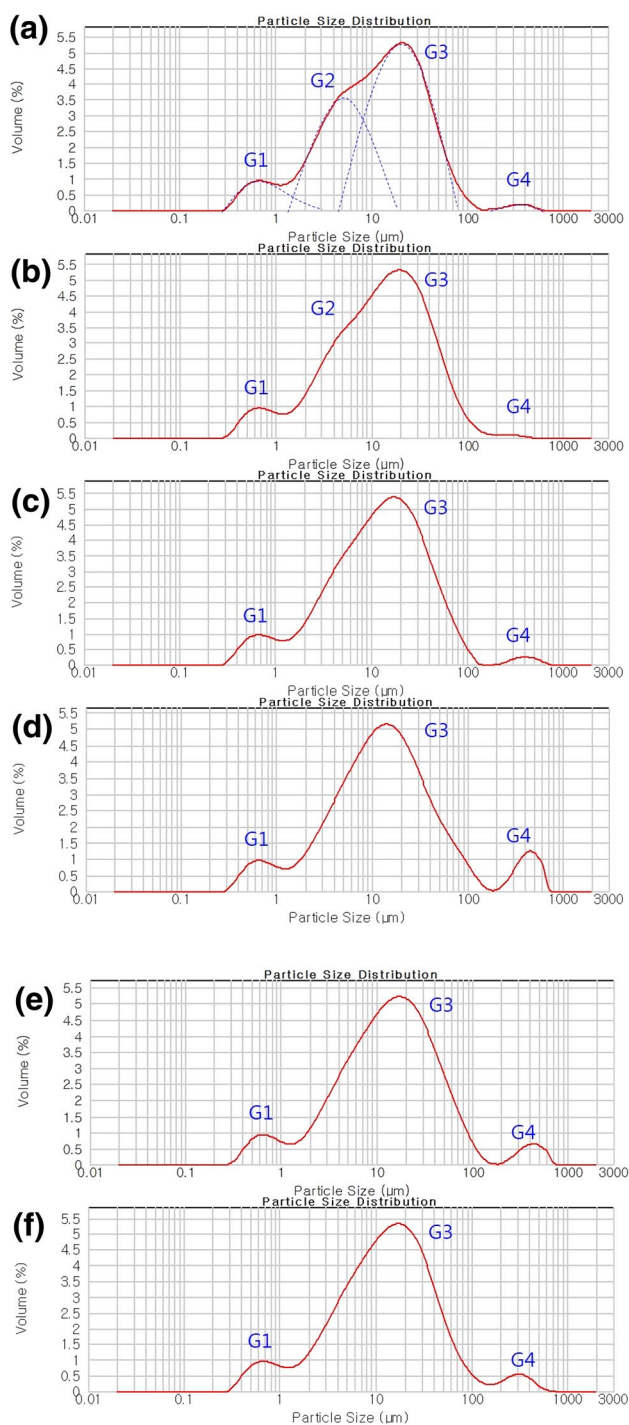


**Fig. 6** Precipitate grain size analysis results; **a** after 1 week, **b** after 2 weeks, **c** after 3 weeks, **d** after 4 weeks, **e** after 5 weeks, and **f** after 6 weeks

G2 represented the stage at which precipitates clumped together and continued to grow; G3 was typical of clumped precipitates dominating the grain-size distribution; and G4, although small in quantity, represented the distribution of the large precipitate particles.

Figure 6b shows the grain size distribution of the precipitates after 2 weeks. G2 had smaller grain sizes than after the first week and displayed a tendency to be absorbed by G3. This occurred because previously generated fine precipitate grains clumped together over time and were incorporated into G3.

Figure 6c shows the grain size distribution of the precipitates after 3 weeks. As precipitate grains gradually grew, G2 ceased to exist and only G3 was present.

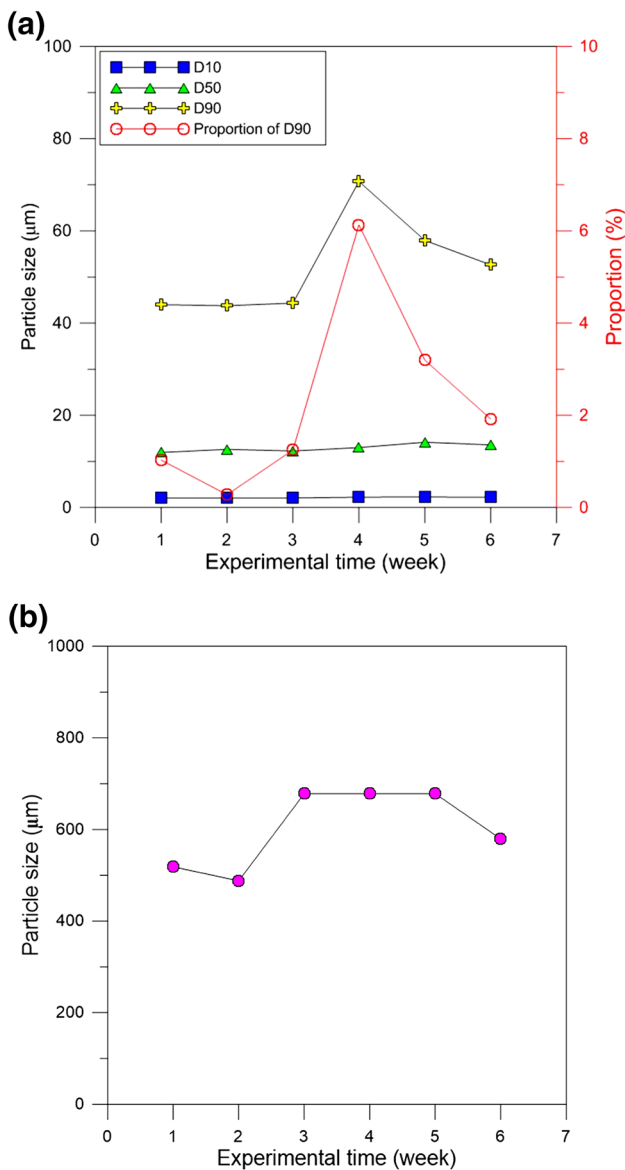
Figure 6d shows the grain size distribution of the precipitates after 4 weeks. By this time, G4 had larger grain sizes than in the third week. This occurred because clumped grains clustered together and gradually grew bigger. The largest precipitate grains were formed after the fourth week. This correlated with the visual inspection, when the membranous precipitates reached their largest size during the fourth week of the experiment.

Figure 6e, f show the grain size distribution of the precipitates after 5 and 6 weeks, respectively. During the fifth and sixth weeks, G4 gradually decreased in size, as the precipitates gradually solidified.

As illustrated in Fig. 6, precipitate size was largest after the fourth week and then gradually decreased in volume and solidified. The greater the volume of the precipitate, the greater its density. After 4 weeks, precipitate volume had reached its maximum, while precipitate density was at its smallest, meaning that the precipitate could be easily swept into the water stream and was suitable for flushing. This is in accordance with the 4-week flushing period recommended by Weaver et al. (2004). However, it should be noted that too frequent flushing could lead to channeling of the organic layer located in the upper portion of the limestone layer.

Figure 7a shows changes in precipitate grain size over time with regard to their D10, D50, and D90 (which correspond to the 10th, 50th, and 90th percentiles respectively of precipitate diameter). The D10 of early grains ranged from 2.0 to 2.3  $\mu\text{m}$ , which is close to the grain size (2.5  $\mu\text{m}$ ) of iron precipitates suggested by Younger et al. (2002). Conversely, D50 showed a tendency to increase from 12.3 to 14  $\mu\text{m}$  after the third week. D90 maintained a grain size of 44  $\mu\text{m}$  during the first 3 weeks, but suddenly increased to 70.7  $\mu\text{m}$  during the fourth week. The proportion of D90 (which is the distribution with the largest grain size) was 1% during the first 3 weeks, more than 6% in the fourth week, and then below 3% after the fifth week. This demonstrated grain growth in the D90 fraction, whose proportion reached its maximum in the fourth week. After the fourth week, the proportion of D90 decreased again due to a decrease in volume caused by gradual solidification of the precipitates.

Figure 7b shows the maximum grain size of the precipitates over time. The maximum grain size was largest ( $\approx 680 \mu\text{m}$ ) after the third week. Assuming the same density conditions and particle shape, the larger the size of the



**Fig. 7** Characteristics of precipitate particles as a function of experimental time; variations of particle-size mean of the D10, D50, and D90 groups based on grain size results and proportion of D90 (a) and maximum particle sizes (b)

particle, the larger the flow velocity required to move the particle. Maximum particle size was therefore an important parameter in determining the critical velocity.

**EDS Analysis**

Table 2 shows the results of the EDS analysis, identifying the chemical composition of each type of precipitate. The iron content was highest in the membranes, intermediate in the botryoidal precipitates, and lowest in the fine grains; the iron content of the white, floating material was below the detection limit. Conversely, the sulfur content was highest

**Table 2** Chemical composition of each precipitation type based on energy dispersive spectrometer (EDS) analysis

Element (wt.%)	Precipitation type			
	Membrane	Botryoidal	Fine-grained	White floating
Fe	51.4	27.5	17.7	–
O	38.0	50.7	52.7	46.3
Ca	0.3	1.9	0.2	28.2
C	3.3	11.5	–	3.9
Si	–	–	0.7	–
S	6.8	7.1	12.7	21.4
Mg	–	0.9	3.6	0.2
Al	0.2	0.4	12.4	–
Total	100.0	100.0	100.0	100.0

– Below detection limit

in the white floating material, followed by the fine grains and botryoidal precipitates, and lowest in the membranes. The chemical composition of the white floating material was similar to gypsum (CaSO<sub>4</sub>).

Visual inspection revealed that the fine-grained and white floating precipitates appeared during the early precipitation stage, while the membrane and botryoidal precipitates were dominant during the later stage. The iron and sulfur content appeared to be related to the precipitate type and the stage in which they appeared.

**SEM Image Analysis**

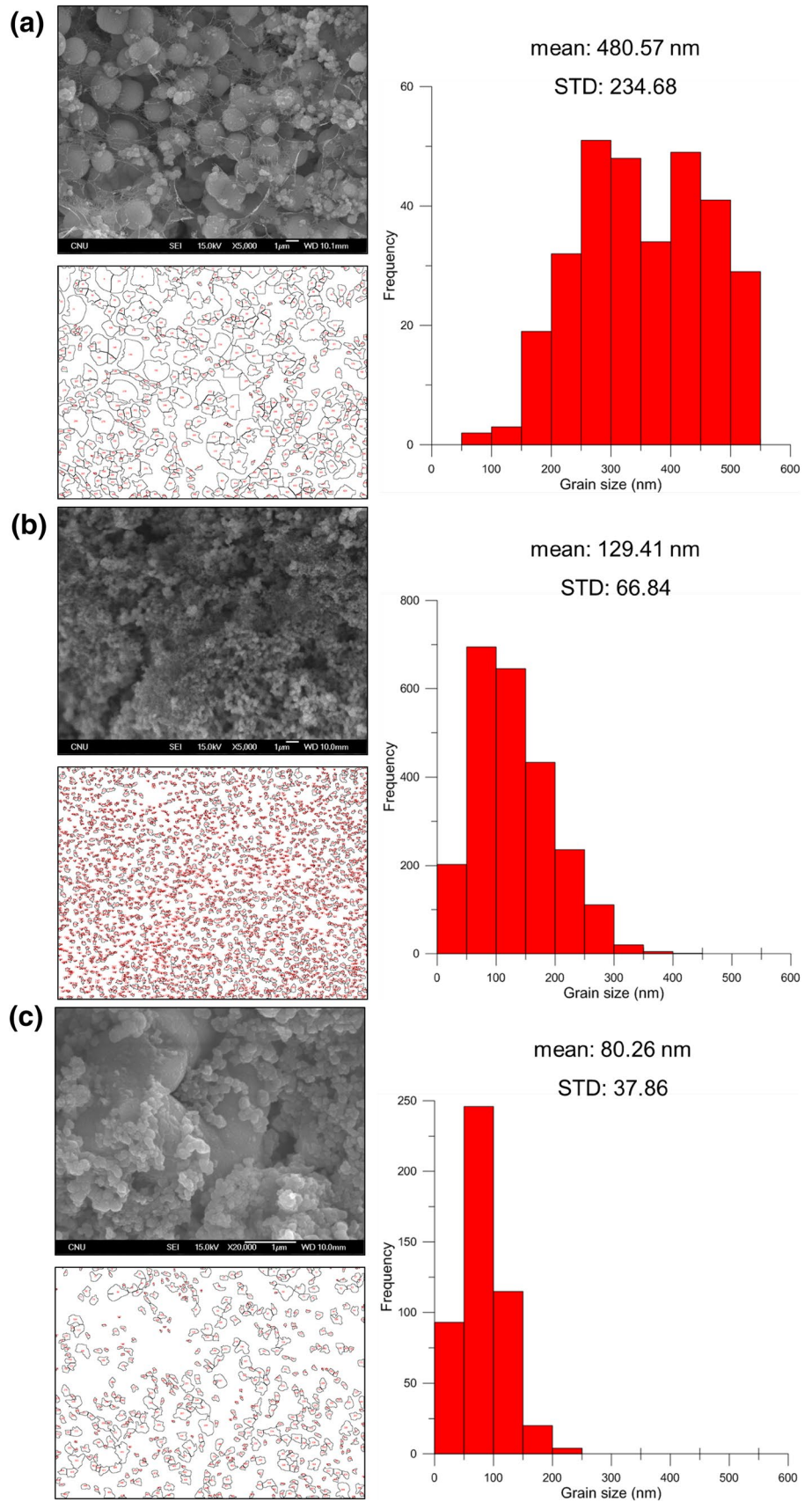
Figure 8 shows the results of the grain size analysis, in which SEM images and Image J software were used to determine the characteristics of the iron oxides (membrane, botryoidal, and fine-grained) at the microscopic scale. The SEM images of the membrane and botryoidal types were analyzed at 5000-fold magnification, and SEM images of the fine-grained type were analyzed at 20,000-fold magnification. The SEM results were different from those of the grain size analysis because the SEM images were analyzed after dehydrating the iron precipitates, while the images for grain-size analysis were obtained from samples without dehydration.

It can be seen in Fig. 8a that the standard deviation and mean grain size of the membrane type was relatively large. Membranous precipitates formed a reticulated material as shown in the figure and through the agglutination of grains. The standard deviation and mean particle size in the botryoidal type were smaller than those of the membrane type (Fig. 8b). Particles formed fine grains loosely distributed along the upper surface of the limestone and their mean particle size was the smallest when compared to the other types (Fig. 8c).

As described previously, membrane type iron oxides grew rapidly during the first 4 weeks and had a large dispersion of



**Fig. 8** SEM image analysis results and grain size histograms of each precipitation type; **a** membrane type, **b** botryoidal type, and **c** fine-grained type



particle distribution. Conversely, fine-grained and botryoidal precipitates grew for a relatively long time and their dispersion was relatively small.

### Critical Velocity

To measure the critical velocity of iron precipitates flowing into the flushing system, it was first necessary to select appropriate precipitates as test subjects. The critical velocity was tested after dehydrating the three types of precipitates. The measured and calculated critical velocities of each precipitate are indicated in Table 3. The diameter of the botryoidal and membrane type precipitates was considered equivalent, i.e. the diameter of a sphere of equivalent area. Fine-grained precipitates had the largest critical velocity (0.12 m/s), while membrane type precipitates, which had the largest area, showed the smallest critical velocity. Depending on shape, membrane type precipitates had a critical velocity between 0.05 and 0.107 m/s (Table 3); the latter being similar to the critical velocity of fine-grained precipitates. Botryoidal precipitates had a critical velocity of 0.063 m/s.

Both membrane and botryoidal precipitates had a lower critical velocity than fine-grained precipitates. In addition, membranous precipitates were thinner but had a wider surface area than botryoidal precipitates, meaning they were subject to greater resistance by the water flow. When compared to fine-grained precipitates, pore volumes of membrane and botryoidal precipitates were larger in proportion to the precipitate volume, causing the apparent density of membrane and botryoidal precipitates to be lower than that of fine-grained precipitates.

Although the density of the precipitate had an important effect on its movement in water, no differences in precipitate density were observed according to precipitate type or time. This is presumably because the density of the precipitate was measured by drying the precipitate. Drying a precipitate that maintains a constant volume in water reduces its volume. Therefore, the volume measured when dry did not represent the volume in water. A new method is needed to accurately measure the volume of precipitate in water.

The measured critical velocities of the botryoidal precipitates were in good agreement with the equations of Oroskar and Turian (1980) and Thomas (1979) when the measured density and equivalent diameter values were applied. The

equation suggested by Oroskar and Turian could also be applied to the fine-grained precipitates. Although this equation is applicable only when the grain diameter exceeds 100 μm, it proved more consistent than Thomas' equation, even when the mean grain diameter of the fine-grained precipitates was 20 μm.

### Minimum Number of Orifices Required in the Lateral Pipes of Flushing Systems

To calculate the minimum number of orifices in lateral pipes needed to ensure that precipitates do not accumulate (but instead move freely), the critical velocity was first calculated using Oroskar and Turian's equation, selecting a maximum grain size (of iron precipitates) of 700 μm, based on Fig. 7b. As a result, the critical velocity of fine-grained precipitates with a diameter of 15 μm was 0.645 m/s. This result falls within the critical velocity range (0.6–0.9 m/s) proposed by Corbitt (1990) for precipitates that do not settle in the header pipe but instead move freely. Taking into account safety factors, it is appropriate to design flushing systems within the critical velocity range proposed by Corbitt (1990). The minimum number of orifices that the lateral pipe should have was calculated via Eq. 3.

$$n_{O_{min}} = \frac{V_{cv}}{V_o} \left( \frac{D_L}{D_o} \right)^2 = \frac{0.645}{V_o} \left( \frac{D_L}{D_o} \right)^2 \tag{3}$$

where,  $n_{O_{min}}$  is the minimum number of orifices,  $V_{cv}$  is the critical velocity of iron precipitates (m/s),  $V_o$  is the average velocity (m/s) of water flowing into the orifices, and  $D_o$  and  $D_L$  are the diameters of the orifices and lateral pipe, respectively. Equation 3 does not consider frictional resistance induced by flow inside the lateral pipe. It should be noted that, for accurate pipe design, the frictional resistance value should be added to the equation.

### Conclusions

In this study, an AMD precipitate growth test revealed that precipitates gradually grow over time until they start to hardening after 4 weeks, when grain size decreases. These results were confirmed by precipitate grain size analysis.

**Table 3** Minimum flow velocities required for precipitate transport by precipitation type acquired

Precipitation type	Equivalent diameter (mm)	Critical velocity (m/s)		
		Measured value	Oroskar and Turian (1980)	Thomas (1979)
Membrane	4.2	0.050	–	–
Botryoidal	2.5	0.063	0.063	0.074
Fine grain	0.2	0.107	0.120	0.540

Precipitates were classified into four types based on shape: membranous, botryoidal, fine-grained, and white floating particles. The fine-grained precipitates were dominant during the early stage of precipitation, while over time, membrane and botryoidal precipitates became dominant. White floating precipitates were always present in the limestone layers not coated by precipitates and had a chemical composition similar to gypsum. While the white floating and fine-grained precipitates had a high sulfur and low iron content, the membrane and botryoidal precipitates had a low sulfur and high iron content.

The results of the critical velocity test of the membrane, botryoidal, and fine-grained precipitates agreed with the critical velocities calculated using the equation suggested by Oroskar and Turian (1980), which was applicable even at particle sizes below 20  $\mu\text{m}$ . The calculated critical velocity of the maximum grain size of the fine-grained precipitates fell within the critical velocity range (0.6–0.9 m/s) proposed by Corbitt (1990). In addition, the minimum number of orifices in lateral pipes in a flushing system needed to prevent precipitate accumulation was determined by applying the calculated critical velocities to Corbitt's equation.

The results of this study improve understanding of the types and characteristics of precipitates in a limestone bed over time. In addition, the maximum critical velocity proposed in this study could be used as the minimum flow velocity needed to move precipitates in a flushing system.

**Acknowledgements** This research was supported by the Basic Research Project of the Korea Institute of Geoscience and Mineral Resources (KIGAM) and Mine Reclamation Corp.(MIRECO), funded by the Ministry of Science and ICT of Korea.

## References

- Akcil A, Koldas S (2006) Acid mine drainage (AMD): causes, treatment and case studies. *J Clean Prod* 14:1139–1145
- Bhattacharya J, Ji S, Lee H, Cheong Y, Yim G, Min J, Choi Y (2008) Treatment of acidic coal mine drainage: design and operational challenges of successive alkalinity producing systems. *Mine Water Environ* 27:12–19
- Christensen B, Laake M, Lien T (1996) Treatment of acid mine water by sulfate-reducing bacteria; results from a bench scale experiment. *Water Res* 30:1617–1624
- Corbitt RA (1990) Standard handbook of environmental engineering. McGraw-Hill, New York City
- Cravotta III CA (2008) Laboratory and field evaluation of a flushable oxic limestone drain for treatment of net-acidic drainage from a flooded anthracite mine. Pennsylvania, USA. *Appl Geochem* 23:3404–3422
- Danehy TP, Hilton T, Watzlaf GR, Johnson F, Busler SL, Denholm CF, Dunn MH (2002) Vertical flow pond piping system design considerations. In: *Proceeding, annual meeting of American Soc of Mining and Reclamation (ASMR)*, pp 916–934
- Demchak J, Morrow T, Skousen J (2001) Treatment of acid mine drainage by four vertical flow wetlands in Pennsylvania. *Geochem Explor Env A* 1:71–80
- Ford KL (2003) Passive treatment systems for acid mine drainage. US Bureau of Land Management. <http://www.blm.gov/nstc/library/techno2.htm>. Accessed 1 Apr 2017
- Hedin RS, Nairn RW, Kleinmann RLP (1994) Passive treatment of polluted coal mine drainage. In: USBM IC 9389. US Dept of the Interior, Washington, DC
- Jarvis AP, Laine DM (2003) Engineering design aspects of passive in situ remediation of mining effluents. *Land Contam Reclam* 11:113–125
- Kepler DA, McCleary EC (1997) Passive aluminum treatment successes. In: *Proceeding, 18th Annual WV Task Force Symp*. <https://wvmdtaskforce.files.wordpress.com/2015/12/97-kepler.pdf>. Accessed 1 Apr 2017
- Lee JY, Kim JH, Woo KJ, Ji WH (2013) A full-scale successive alkalinity-producing passive system (SAPPS) for the treatment of acid mine drainage. *Water Air Soil Poll*. <https://doi.org/10.1007/s11270-013-1656-4>
- Naver (2016) <https://map.naver.com>. Accessed 3 May 2016
- Oroskar AR, Turian RM (1980) The critical velocity in pipeline flow of slurries. *AIChE J* 26:550–558
- Rose AW (2004) Vertical flow systems – effects of time and acidity relations. In: *Proceedings, National Meeting of the American Soc of Mining and Reclamation (ASMR) and the 25th WV surface mine drainage task force*, pp 1595–1616
- Rose AW (2006) Long-term performance of vertical flow ponds—an update. In: *Proceeding, 7th international conf on acid rock drainage (ICARD)*, pp 1595–1616
- Skousen J, Zipper CE, Rose A., Nairn R, McDonald LM, Kleinmann RL, Ziemkiewicz PF (2017) Review of passive systems for acid mine drainage treatment. *Mine Water Environ* 36:133–153
- Taylor K, Banks D, Watson I (2016) Characterisation of hydraulic and hydrogeochemical processes in a reducing and alkalinity-producing system (RAPS) treating mine drainage. South Wales, UK. *Int J Coal Geol* 164:35–47
- Thomas AD (1979) Predicting the deposit velocity for horizontal turbulent pipe flow of slurries. *Int J Multiphas Flow* 5:113–129
- Watson IA, Taylor K, Sapsford DJ, Banks D (2009) Tracer testing to investigate hydraulic performance of a RAPS treating mine water in south Wales. In: *Proceeding 8th ICARD (Securing the Future)*, pp 762–771
- Watzlaf GR, Kairies CL, Schroeder KT, Danehy T, Beam R (2002) Quantitative results from the flushing of four reducing and alkalinity-producing systems. Presented at the WV Surface Mine Drainage Task Force Symp. <https://wvmdtaskforce.files.wordpress.com/2016/01/02-watzlaf.pdf>. Accessed 1 Apr 2017
- Weaver KR, Lagnese KM, Hedin RS (2004) Technology and design advances in passive treatment system flushing. In: *Proceedings of annual meeting of ASMR and the 25th WV surface mine drainage task force*, pp 1974–1989
- Wolkersdorfer C, Hasche A, Gobel A, Younger PL (2005) Tracer test in the Bowden Close passive treatment system. *Wiss Mitt* 28:87–92
- Yim GJ, Ji SW, Cheong YW, Carmen MN, Song HC (2015) The influences of the amount of organic substrate on the performance of pilot-scale passive bioreactors for acid mine drainage treatment. *Environ Earth Sci* 73:4717–4727
- Younger P (2000) The adoption and adaptation of passive treatment technologies for mine waters in the United Kingdom. *Mine Water Environ* 19:84–97
- Younger P, Banwart S, Hedin R (2002) *Mine water hydrology*. Springer, Netherlands